INTERNATIONAL JOURNAL FOR NUMERICAL METHODS IN FLUIDS
Int. J. Numer. Meth. Fluids 2004; **46**:19–35 (DOI: 10.1002/fld.744)

Numerical calculations of erosion in an abrupt pipe contraction of different contraction ratios

M. A. Habib*,†,‡, H. M. Badr‡, R. Ben-Mansour§ and S. A. M. Said‡

Mechanical Engineering Department, King Fahd University of Petroleum & Minerals, Dhahran 31261, Saudi Arabia

SUMMARY

Erosion predictions in a pipe with abrupt contraction of different contraction ratios for the special case of two-phase (liquid and solid) turbulent flow with low particle concentration are presented. A mathematical model based on the time-averaged governing equations of 2-D axi-symmetric turbulent flow is used for the calculations of the fluid velocity field (continuous phase). The particle-tracking model of the solid particles is based on the solution of the governing equation of each particle motion taking into consideration the effect of particle rebound behaviour. Models of erosion were used to predict the erosion rate in mg/g. The effect of Reynolds number and flow direction with respect to the gravity was investigated for three contraction geometries considering water flow in a carbon steel pipe. The results show that the influence of the contraction ratio on local erosion is very significant. However, this influence becomes insignificant when the average erosion rates over the sudden contraction area are considered. The results also indicate the significant influence of inlet velocity variations. The influence of buoyancy is significant for the cases of low velocity of the continuous flow. A threshold velocity below which erosion may be neglected was indicated. Copyright © 2004 John Wiley & Sons, Ltd.

KEY WORDS: erosion; pipe contraction; numerical calculation; contraction ratios

1. INTRODUCTION

When solid particles are transported in a fluid flow, erosion may occur and may cause equipment malfunctioning (vibration, leakage, excessive energy losses, etc.) and may also lead to complete failure of machine components. Abrupt pipe contraction is experienced in various gas and liquid flow passages such as flow in pipes and pipe fittings (valves, bends, elbows, flow meters, etc.), flow in pumps, turbines, compressors and many others. Accu-

*Correspondence to: M. A. Habib, Mechanical Engineering Department, King Fahd University of Petroleum & Minerals, Dhahran 31261, Saudi Arabia.
†E-mail: mahabib@kfupm.edu.sa
‡Professor.
§Assistant professor.

Contract/grant sponsor: King Fahd University of Petroleum and Minerals

Published online 14 July 2004

Received 21 June 2003
Revised 16 April 2004

rate prediction of the rate of erosion in a specific application is one of the very complicated problems since it requires detailed investigation of the solid particle motion before and after impact. The difficulty arises mainly from the fact that most flows occurring in industrial processes are turbulent which makes the particle trajectory and impact characteristics difficult to predict taking into consideration all fluid forces acting on the particle. The following literature review is limited to previous work done on erosion in pipes and pipe fittings.

The use of computational methods in erosion prediction constitutes a combination of flow modelling, Lagrangian particle tracking, and the use of erosion correlations. The flow model is used to determine the flow field for a given geometry while the particle tracking model is used to determine the particle trajectories for solid particles released in the flow. The particle impingement information extracted from the trajectories is used along with the empirical erosion equations to predict the erosion rates. This model, which is sometimes called the Lagrangian approach, requires expertise in fluid dynamic modelling and a large amount of computational work. Numerical solutions for the turbulent flow of an air–solid suspension in a heated vertical pipe using Eulerian–Eulerian and Eulerian–Lagrangian formulations were conducted [1]. The main task was to assess the accuracy of these two formulations, taking the experimental data reported by Tsuji *et al.* [2] and Jepson *et al.* [3] as a base for comparison. The first part of the pipe contains developing flow with no heat transfer. In the second part of the pipe, the dynamically fully developed flow was heated using a heated section of the pipe (constant heat flux). The simulation was carried out for different values of mass loading with particles of 500 μm diameter. The comparisons with experimental data for the dynamic features of the flow showed the same accuracy level for both formulations, especially for dilute flows. However, the accuracy was found to decrease significantly in both formulations as more particles were injected in the flow.

The application of Lagrangian models was considered by Lu *et al.* [4], Keating and Nesic [5], Edwards *et al.* [6], Wallace *et al.* [7] and Wang *et al.* [8] who used combinations of computational fluid dynamics and different Lagrangian particle tracking models to predict the particle movement through complex geometries. Different computational fluid dynamic (CFD) packages such as PHOENICS [5, 9], CFD code [6] and CFX-code [10] were used to predict the fluid flow field. Wang *et al.* [8] developed a computational model for predicting the rate of erosive wear in a 90° elbow for the two cases of sand in air and sand in water. The flow field was first obtained and then the particle trajectory and impacting characteristics were determined by solving the equation of particle motion taking into consideration all the forces including drag, buoyancy, and virtual mass effects with the assumption of a uniform distribution of the solid particles at the starting section. The penetration rate was obtained using a semi-empirical relation that was previously developed [11]. A comparison between the predicted penetration rates and the available experimental data showed a good agreement.

Shirazi and McLaury [12] presented a model for predicting multiphase erosion in elbows. The model was developed based on extensive empirical information gathered from many sources, and it accounts for the physical variables affecting erosion, including fluid properties, sand production rate and size, and the fluid-stream composition. An important different feature of this model was the use of the characteristic impact velocity of the particles. The method used for obtaining this characteristic velocity for an elbow was an extension of a previous method introduced by the same authors for the case of a single-phase flow. The

results from the model were compared with previous experimental results for elbows and were found to have a better agreement with data related to failure in elbows in industrial fields.

In the study of Edwards *et al.* [6], an erosion prediction procedure was developed and verified based on a CFD code combining flow field analysis and particle tracking for obtaining particle impingement data. The erosion rate was then computed using the empirical relations of Ahlert [11] and applied to predict erosion in a pipe bend fitting made of carbon steel. The CFD code utilized a finite-volume multi-block approach for solving Navier–Stokes equations based on a user-defined computational model that was described by Patankar [13]. The authors used the Lagrangian particle-tracking algorithm of the CFD code for the prediction of individual trajectories of the dispersed phase through the flow field.

Based on the above literature search and to the best of the authors' knowledge, most of the published work on erosion in pipes focused on straight pipes and pipe fittings such as bends and elbows. The erosion process occurring in an abrupt pipe contraction or sudden enlargement was not considered in any previous study. The present research work aims at studying the effect of fluid flow parameters and contraction ratios on the rate of erosion in pipe contractions under conditions simulating the actual working conditions. The calculation of the flow pattern and solid particle motion inside the pipe contraction was performed and the available data in the literature are used for estimating the rate of erosion.

2. THE CALCULATION PROCEDURE

The rate of erosion in tubes depends upon many parameters such as the properties of the impacting particles, the properties of the tube material, and the other parameters of the impact process [14–16]. Thus, the flow field characteristics and the details of the particle impact process as well as the erosion rate correlations are required for the prediction of the rate of erosion in tubes. In the present work, the flow velocity field in the domain of interest was predicted. This is followed by the calculation of the trajectories of solid particles entrained in the fluid using Lagrangian particle tracking model and then extract the particle impact data. Finally, the erosion and penetration rates were predicted based on the available formulae [7].

The Lagrangian particle tracking method represents a one-way flow-to-particle coupling method that can be used when low volume of particles is simulated. Two computational models were developed. The first is the continuous phase model (dealing with the prediction of the flow velocity field) and the second is the particle tracking model (dealing with the prediction of particle motion). A brief discussion of the two models is presented in the following sections.

2.1. The continuous phase model

A combination of computational fluid dynamics and Lagrangian particle tracking is normally used to predict the particle movement through complex geometries [5–8]. To predict the flow pattern of the continuous flow phase, the conservation equations for mass and momentum are solved. Additional transport equations for the turbulence model are also solved since the flow is turbulent. The time-averaged governing equations of 3-D turbulent flow can be found in many references [17, 18] and can be presented as follows.

2.1.1. The continuity and momentum equations. Mass conservation: The steady-state time-averaged equation for conservation of mass can be written as

$$\frac{\partial}{\partial x_j}(\rho \overline{U_j}) = 0 \tag{1}$$

Momentum conservation: The steady-state time-averaged equation for the conservation of momentum in the i direction can be expressed as

$$\frac{\partial}{\partial x_j}(\rho \overline{U_i U_j}) = -\frac{\partial p}{\partial x_i} + \frac{\partial}{\partial x_j}\left(\mu \frac{\partial \bar{u}_i}{\partial x_j}\right) - \frac{\partial}{\partial x_j}(\rho \overline{u_i u_j}) \tag{2}$$

where p is the static pressure. The stress tensor $\rho \overline{u_i u_j}$ is given by

$$-\rho \overline{u_i u_j} = \left[\mu_{\text{eff}}\left(\frac{\partial \overline{U_i}}{\partial x_j} + \frac{\partial \overline{U_j}}{\partial x_i}\right)\right] - \frac{2}{3}\rho k \delta_{ij} \tag{3}$$

where δ_{ij} is the Kronecker delta which is equal to 1 for $i = j$ and equals 0 for $i \neq j$ and $\mu_{\text{eff}} = \mu_t + \mu$ is the effective viscosity. The turbulent viscosity, μ_t, is calculated using the high-Reynolds number form as

$$\mu_t = \rho C_\mu \frac{k^2}{\varepsilon} \tag{4}$$

with $C_\mu = 0.0845$, k and ε are the kinetic energy of turbulence and its dissipation rate. These are obtained by solving their conservation equations as given below.

2.1.2. Conservation equations for the turbulence model. The conservation equations of the turbulence model [19, 20] are given as follows:

The kinetic energy of turbulence:

$$\frac{\partial}{\partial x_j}(\rho \overline{U_j} k) = \frac{\partial}{\partial x_j}\left(\frac{\mu_{\text{eff}}}{\sigma_k} - \frac{\partial k}{\partial x_j}\right) + G_k - \rho\varepsilon \tag{5}$$

The rate of dissipation of the kinetic energy of turbulence:

$$\frac{\partial}{\partial x_j}(\rho \overline{U_j} \varepsilon) = \frac{\partial}{\partial x_i}\left(\frac{\mu_{\text{eff}}}{\sigma_\varepsilon}\frac{\partial \varepsilon}{\partial x_i}\right) + C_1 G_k \frac{\varepsilon}{k} - C_2^* \rho \frac{\varepsilon^2}{k} \tag{6}$$

where G_k represents the generation of turbulent kinetic energy due to the mean velocity gradients and is given by

$$G_k = -\rho \overline{u_i u_j} \frac{\partial \overline{U_j}}{\partial x_i} \tag{7}$$

The quantities σ_k and σ_ε are the effective Prandtl numbers for k and ε, respectively, and C_2^* is given by Shih *et al.* [20] as

$$C_2^* = C_2 + C_3 \tag{8}$$

where C_3 is a function of the term k/ε and, therefore, the model is responsive to the effects of rapid strain and streamline curvature and is suitable for the present calculations. The model constants C_1 and C_2 have the values; $C_1 = 1.42$ and $C_2 = 1.68$.

The wall functions establish the link between the field variables at the near-wall cells and the corresponding quantities at the wall. These are based on the assumptions introduced by Launder and Spalding [21] and have been most widely used for industrial flow modelling. The details of the wall functions are provided by the law-of-the-wall for the mean velocity [17].

2.1.3. Boundary conditions. The velocity distribution is considered fully developed turbulent pipe flow at the inlet section with the velocity in the direction of the nozzle axis. Kinetic energy and its dissipation rate are assigned through a specified value of $\sqrt{k/\bar{U}^2}$ equal to 10% and a length scale L, equal to the diameter of the inlet pipe. The boundary condition applied at the exit section is that of fully developed flow. At the wall boundaries, all velocity components are set to zero in accordance with the no-slip and impermeability conditions. The value of the kinetic energy of turbulence near the wall, k_p, is calculated from the transport equation for k with flux of energy to the solid wall is set to zero. The corresponding value of ε is calculated from $\varepsilon = c_\mu k^{3/2}/l$ with l is given as $l = c_\mu^{1/4} \kappa y_p$ where κ is constant and is equal to 0.42. y_p is the distance of the node adjacent to the wall.

2.1.4. Solution procedure. The conservation equations are integrated over a typical volume that is formed by division of the flow field into a number of finite volumes, to yield the solution. The equations are solved simultaneously using the solution procedure described by Patankar [13]. Calculations are performed with at least 300 000 elements considering fine elements in the section of the pipe contraction close to the inlet to small pipe. Convergence is considered when the maximum of the summation of the residuals of all the elements for U_i $(i = 1, 2)$ and pressure correction equations is less than 0.1%. The grid independence tests were performed by increasing the number of control volumes from 260 000 to 380 000 in two steps; 260 000–320 000 and 320 000–380 000. The influence of refining the grid on the velocity field is very negligible and indicates that more mesh refinement will result in negligible changes in the results of the computational model.

2.2. Particle tracking

The particle tracking calculation is required to determine the particle trajectory from the moment it enters the pipe until it leaves the small tube. Of special interest is the particle velocity (magnitude and direction) before every impact either on the pipes walls or anywhere on the tube sheet. Such impact velocity is not only important for the calculation of solid surface erosion but also in the determination of the particle trajectory during its course of motion following impact. One of the main assumptions in this study is that the solid particles are not interacting with each other (the particles do not collide and the motion of any particle is not influenced by the presence or motion of neighbouring particles). Moreover, the influence of particle motion on the fluid flow field is considered very small and can be neglected. These two assumptions are based on the condition of fairly dilute particle concentration. The same assumptions were made by Lu *et al.* [4], Keating and Nesic [5], Edwards *et al.* [6], Wallace *et al.* [7], Benchaita *et al.* [22] and Shirazi *et al.* [23] in the solution of similar problems of low particle concentration (less than 2–3% by weight). Taking the main hydrodynamic forces

into consideration, the particle equation of motion can be written [7] as

$$\frac{\mathrm{d}\underline{u}_\mathrm{p}}{\mathrm{d}t} = F_\mathrm{D}(\underline{u} - \underline{u}_\mathrm{p}) + \underline{g}(\rho_\mathrm{p} - \rho)/\rho_\mathrm{p} + \underline{F}_\mathrm{vm} + \underline{F}_\mathrm{pg} + F_\mathrm{sl} \tag{9}$$

where $F_\mathrm{D}(\underline{u} - \underline{u}_\mathrm{p})$ is the drag force per unit particle mass and $F_\mathrm{D} = 3C_\mathrm{D}\mu Re_\mathrm{p}/(4\rho_\mathrm{p}D_\mathrm{p}^2)$, $\underline{g}(\rho_\mathrm{p}-\rho)/\rho_\mathrm{p}$ is the buoyancy force term, $\underline{F}_\mathrm{vm}$ is the virtual mass term (force required to accelerate the fluid surrounding the particle), $\underline{F}_\mathrm{pg}$ is the pressure gradient term and $\underline{F}_\mathrm{sl}$ is the Saffman lift force or lift due to shear. The Magnus lift force (resulting from particle rotation) was neglected because it is only important at low Reynolds number which is not the case for the present calculations. The Basset history force (the force accounting for the flow field unsteadiness) has been neglected due to low particle acceleration in the present flow field calculations.

The particle Reynolds number, Re_p, and the drag coefficient, C_D, are obtained from

$$Re_\mathrm{p} = \frac{\rho D_\mathrm{p}|\underline{u}_\mathrm{p} - \underline{u}|}{\mu} \tag{10}$$

$$C_\mathrm{D} = a_1 + \frac{a_2}{Re_\mathrm{p}} + \frac{a_3}{Re_\mathrm{p}^2} \tag{11}$$

where the a's are constants given by Morsi and Alexander [24] for smooth spherical particles over several ranges of Re_p. Another equation that is frequently used for C_D [25] is given by

$$C_\mathrm{D} = \frac{24}{Re_\mathrm{p}}(1 + b_1 Re_\mathrm{p}^{b_2}) + \frac{b_3 Re_\mathrm{p}}{b_4 + Re_\mathrm{p}} \tag{12}$$

where b_1, b_2, b_3 and b_4 are expressed in terms of the surface area of a sphere having the same volume as the particle to the actual surface area of the particle.

In the present case of low particle concentration, the particles motions are considered non-interacting and the dominant force in Equation (9) is the drag force [6]. Some of the other forces given in Equation (9) are of small order of magnitude and can be neglected in this study. The first of these is the virtual mass term that takes care of the force required to accelerate the fluid surrounding the particle. This term can be expressed as

$$\underline{F}_\mathrm{vm} = \frac{1}{2}\frac{\rho}{\rho_\mathrm{p}}\frac{\mathrm{d}}{\mathrm{d}t}(\underline{u} - \underline{u}_\mathrm{p}) \tag{13}$$

and is important when $\rho > \rho_\mathrm{p}$ which is not the case in the present study. The second force is that due to pressure gradient, $\underline{F}_\mathrm{pg}$, that arises from the influence of the pressure gradient in the flow which acts on every volume element of the flowing medium and can be written as

$$\underline{F}_\mathrm{pg} = \left(\frac{\rho}{\rho_\mathrm{p}}\right)\underline{\nabla} p \tag{14}$$

The above statement implies that the pressure does not vary significantly over a distance of one particle diameter, a condition that is normally satisfied for reasonably small particles. Accordingly, the pressure gradient force is neglected in the present study not only due to the small size of the particles but also due to the small pressure gradient prevailing in the flow field. The other forces include the thermophoretic force which is related to small particles

suspended in a gas that has a temperature gradient. The particles under such circumstances experience a force in the direction opposite to that of the gradient. Brownian force [26] apply for sub-micron particles. These forces are neglected in the present study. It has been shown by Wallace *et al.* [7] and Meng *et al.* [27] that Saffman's lift force does not contribute greatly to the particle motion and, therefore, it is also neglected in the present calculations.

The particle trajectory equations are solved by stepwise integration over discrete time steps. Integration in time of the equation of particle motion yields the velocity of the particle at each point along the trajectory, with the trajectory itself predicted by:

$$\frac{\mathrm{d}\underline{r}}{\mathrm{d}t} = \underline{u}_{\mathrm{p}} \tag{15}$$

where $\underline{r}$ is the position vector. The above equation is integrated in each co-ordinate direction to predict the trajectories of the discrete phase. During the integration, the fluid phase velocity, $\underline{u}$, is taken as the velocity of the continuous phase at the particle position.

The boundary conditions considered when a particle strikes a boundary surface depends on the nature of that surface and the particle being (i) reflected via an elastic or inelastic collision, (ii) escaped through the boundary or (iii) trapped at the wall. (i) Regarding the reflection via an elastic or inelastic collision, the coefficient of restitution is taken as 0.9 in the present calculations for the cases of reflection at a wall or at an axis of symmetry. The coefficient of restitution defines the amount of momentum in the direction normal to the wall that is retained by the particle after colliding with the boundary [28]. (ii) When the particle encounters such a boundary, it is considered that the particle has escaped and the trajectory calculations are then terminated. (iii) The trajectory calculations for some particles (normally very few particles) are terminated when the particles get trapped in the flow field. This is found to occur when a particle circulates in a confined flow zone. In such a case, the trajectory calculations are terminated.

2.3. The erosion model

The previous experimental results [16, 29] show that the erosive wear-rate exhibits a power-law velocity dependence. The velocity exponent ranges from 1.9 to 2.5. The results also indicate that the erosion rate is a function of the angle of impact. It is shown that the influence of the angle of impact depends greatly on the type of material being brittle or ductile. Prediction of erosion in straight pipes, elbows and tees show the strong influence of fluid properties, sand size and flow velocity on the rate of erosion [30–32]. Erosion is defined as the wear that occurs when solid particles entrained in a fluid stream strike a surface.

There have been many attempts in the past to represent the solid particle erosion process by an analytical formula that could be used to predict erosion under any condition. The complexity of the erosion process and the number of factors involved has meant that no generally applicable equation has been forthcoming. Almost all of the formulae generated have therefore some degree of dependence on empirical coefficients provided by various experimental erosion tests. No definitive theory of erosion currently exists, however, a number of qualitative and quantitative models do exist. These are described in References [5, 6, 8, 12, 33, 34].

The empirical erosion equations suggested by Neilson and Gilchrist [35] were used by Wallace *et al.* [7] to correlate the experimental erosion data to provide an erosion modelling technique. The following formulae [7] proved to provide good results as compared to the

experimental data:

$$E = \frac{1}{N_p}\left\{\frac{\frac{1}{2}u_p^2\cos^2\alpha\sin 2\alpha}{\gamma} + \frac{\frac{1}{2}u_p^2\sin^2\alpha}{\sigma}\right\} \quad \alpha \leqslant 45^\circ \tag{16}$$

$$E = \frac{1}{N_p}\left\{\frac{\frac{1}{2}u_p^2\cos^2\alpha}{\gamma} + \frac{\frac{1}{2}u_p^2\sin^2\alpha}{\sigma}\right\} \quad \alpha > 45^\circ \tag{17}$$

γ and σ are the cutting wear and deformation wear coefficients $\gamma = 33316.9$, $\sigma = 77419.7$ for low velocity [7]. These formulae are used in the present calculations of the erosion rate.

Through the tracking model, impingement information is gathered as particles impinge the walls of the geometry. As particle trajectories are computed, this impingement information is recorded and erosion is computed using empirical relations. Knowledge of the particle impact speed and impact angle allows the erosion rate to be computed. The ability to predict erosion was provided by the authors through FORTRAN subroutines that are used along with the CFD code.

3. RESULTS AND DISCUSSION

3.1. Validation

The erosion results are evaluated in comparison with previous results in order to provide validation of the calculation procedure. Unfortunately, experimental data of erosion rates in pipe contractions and even in pipe flows are not available. The only available data are the calculations of the penetration rate which are provided by McLaury *et al.* [36] for pipe flows. Therefore, calculations considering random (turbulent) impingement rather than direct impingement were performed in a pipe flow. The calculations were made for pipe diameter of 0.1 m, particle diameter of 300 μm and particle density is 2650 kg/m^3. The fluid is water at 60°C and the sand rate is 1 cm^3/s. The pipe material is carbon steel. The results of the calculations as well as the experimental data are presented in terms of the local penetration rate. The local penetration rate represents the depth of wear at various locations on the solid surface. The mass loss for all solid particle impingements was compiled to generate the local penetration rate for each boundary cell. At any given boundary cell, the local penetration rate, P_n, was calculated using the following equation [37, 38]:

$$P_n = 1.24 \times 10^9 \times \frac{\dot{s}}{\rho_m N_p A} E_{lc} \tag{18}$$

where A is the impingement area (m^2), E_{lc} is the local erosion rate (mg/g), N_p is the total number of particles being tracked, P_n is the penetration rate (mil/year), $\dot{s}$ is the sand rate (kg/s) and ρ_m is the density of target material (kg/m^3).

Figure 1 shows the comparison of the penetration rate utilizing the present calculation procedure with the results of the simplified model of McLaury *et al.* [36]. The figure indicates reasonable agreement between the present calculations for straight pipe flows and those of McLaury *et al.* [36] at low velocity values. At the high velocity values, the discrepancy reaches 60% at 15m/s. It may be noted that the calculations of McLaury *et al.* [36] incorporated a very

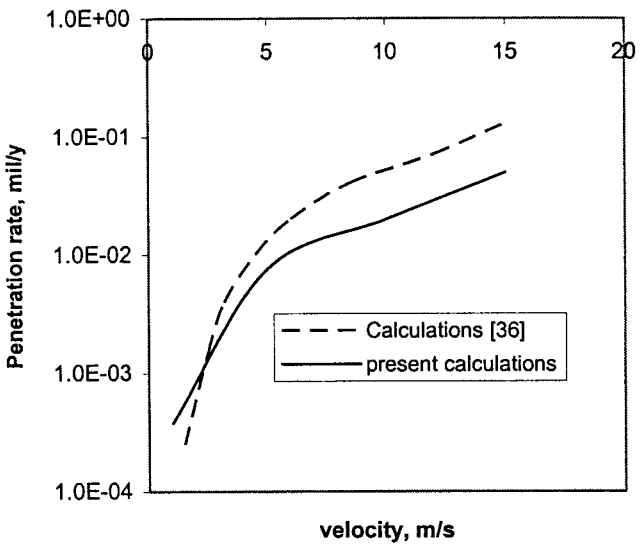

Figure 1. Influence of inlet flow velocity on the penetration rate in a pipe. Flow, water at 60°C; particle size, 300 μm; pipe material, carbon steel; pipe diameter, 10 cm.

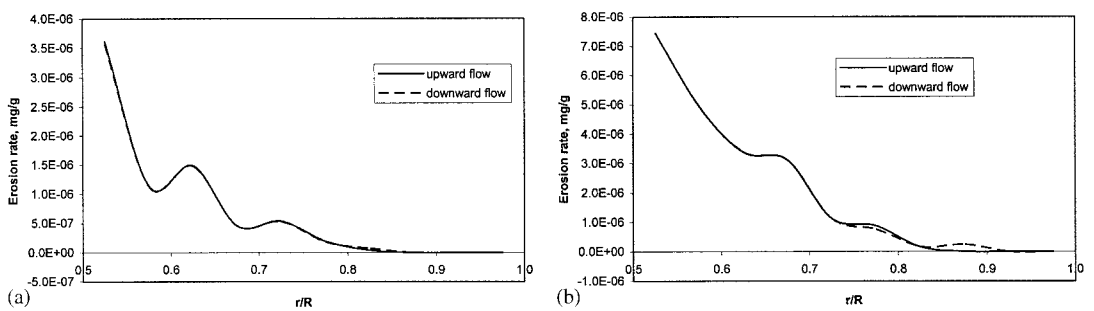

Figure 2. The influence of flow direction on the local rate of erosion; $d/D = 0.5$, $V_i = 10\,\mathrm{m/s}$: (a) Particle diameter = 200 μm; and (b) particle diameter = 400 μm.

simplified model in which the fluctuating velocity components at the sub-layer buffer region (close to the wall and away from the turbulent core) were estimated from the velocity profile of the fully developed pipe flow. The ratio of the number of the particles that impact the tube surface to the amount of the sand flowing in the pipe was estimated via empirical models.

3.2. Influence of inlet flow velocity

The calculations were performed inside the pipe contractions. Three geometries of d/D of 0.25, 0.5 and 0.75 were considered with a fixed inlet diameter of 0.2 m. Two flow configurations, namely upward flow and downward flow, were considered. The particle diameters that were considered in the present study are 10, 100, 200, and 400 μm.

Figure 2 presents the local erosion rate along the contraction plate radius for two different particle sizes 200 and 400 μm at an inlet velocity of 10 m/s and contraction diameter ratio of

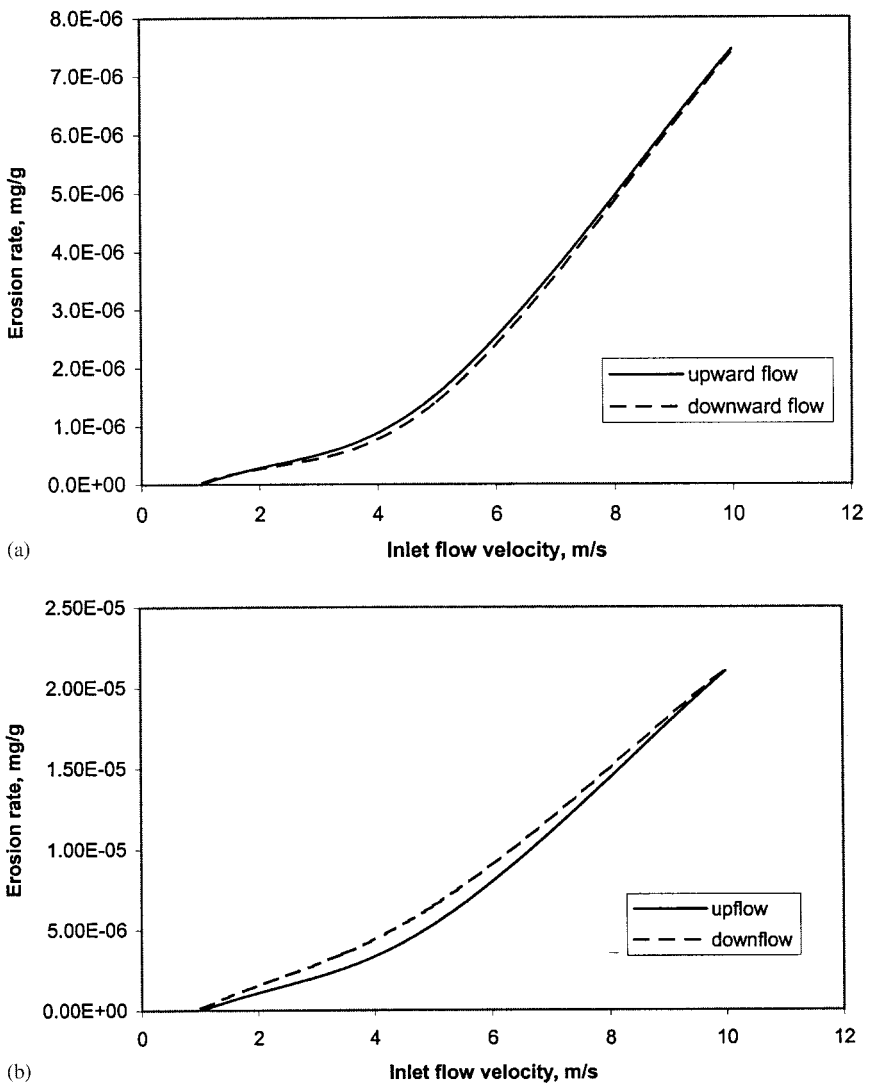

Figure 3. The influence of flow direction and flow inlet velocity on the rate of erosion; $d/D = 0.5$: (a) Particle diameter = 200 μm; and (b) particle diameter = 400 μm.

0.5. The figure exhibits almost similar local erosion distribution for the up- and down-flow cases at both of the considered particle sizes. The figure also indicates higher erosion rates close to the inner tip of the contraction disc for both particle diameters with significantly higher values in the case of the larger particle size. Figure 3 presents the influence of the inlet flow velocity on the erosion rate for two different particle sizes of 200 and 400 μm. The erosion rate is almost tripled as the particle size is doubled. The erosion rate increases

exponentially with the velocity, the figure also provides a comparison of the erosion rate for the two cases of upward and downward flow and exhibits similar distribution with deviations in erosion values between the two cases only at $V_i = 5\,\mathrm{m/s}$. A threshold velocity below which the erosion rate may be avoided can be indicated from the figure. In both cases of 200 and 400 μm, this velocity is around 1 m/s.

3.3. *Influence of the contraction ratio*

The local erosion rate along the radius of the contraction disc is given in Figure 4 for the case of the downward flow at three different contraction ratios of 0.25, 0.5 and 0.75. The figures indicate an erosion free region close to the outside corner where the flow velocity is very small. In this region, there is no impact of particles on the surface. In general, the local erosion rate is increased sharply with the increase in the velocity. The maximum local erosion

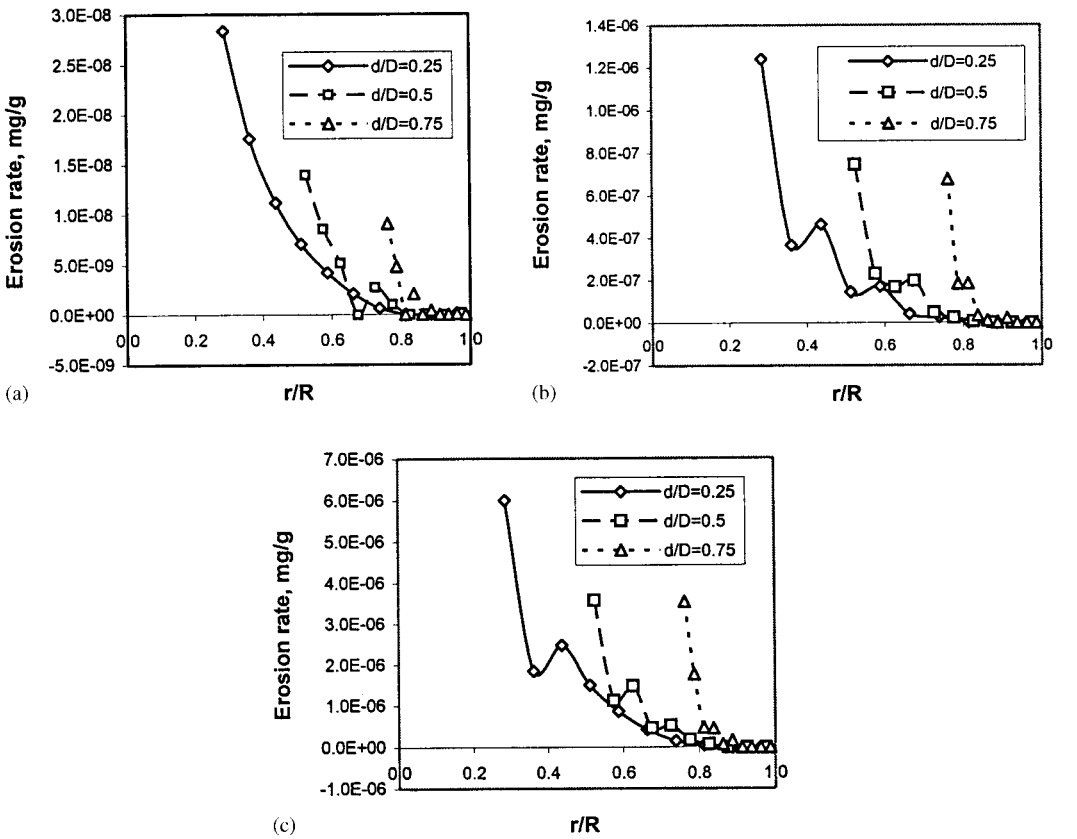

Figure 4. The influence of contraction ratio and inlet flow velocity on the local rate of erosion for the downward flow case, particle diameter = 200 μm: (a) Inlet flow velocity = 1 m/s; (b) inlet flow velocity = 5 m/s; and (c) inlet flow velocity = 10 m/s.

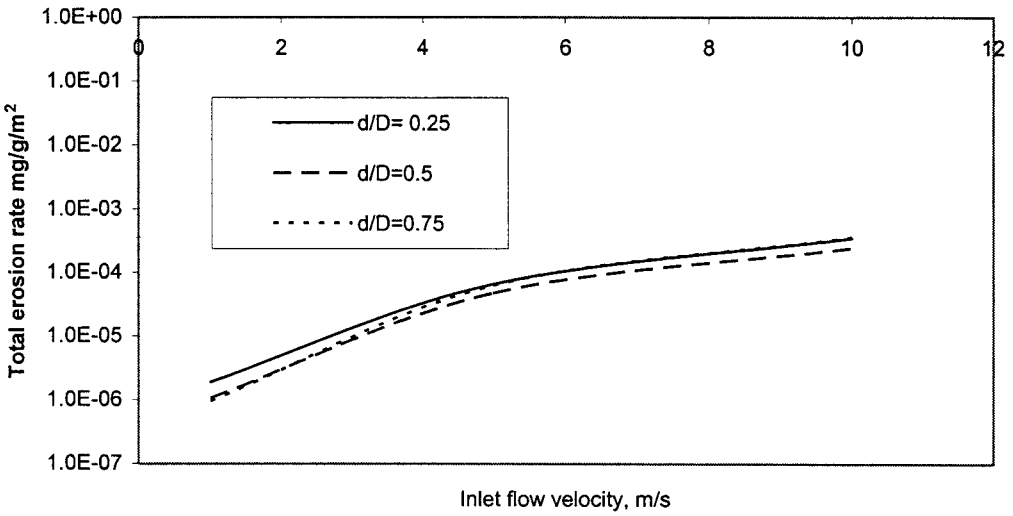

Figure 5. The influence of contraction ratio and inlet flow velocity on the total rate of erosion for the downward flow case, particle diameter = 200 μm.

rate is shown to occur at the inner tip of the contraction. It is also noted that the maximum local erosion rate is increased with decreased contraction ratio. It is indicated that the region of negligible erosion close to the outside corner is of the same size for all the contraction ratios. However, decreasing d/D causes more deflection of the streamlines. The particles do not normally follow these streamlines and, therefore, cause impact on the wall causing high rate of erosion.

The data of Figure 4 was integrated to provide the total erosion rate along the contraction disc and the results are given in Figure 5. The figure presents the influence of the inlet flow velocity on the total erosion rate for the downward flow case at the different values of contraction ratios. In order to eliminate the effect of the disc area, the erosion rate is presented per unit area of the contraction disc. The figure indicates the significant influence of the velocity. It is also shown that a criterion for the threshold inlet velocity below which erosion rate may be negligible can be obtained. Considering the erosion rate per unit area of the contraction disc, it is shown that the influence of the contraction ratio on the erosion rate is insignificant with the ratio of $d/D = 0.5$ giving slightly less erosion rate at the flow inlet velocities of higher values.

Similar to the case of downward flow, the influence of the contraction ratio on the radial distribution of the local erosion rate for the upward flow is presented in Figure 6. Similar observations regarding maximum local erosion and its radial position. However, in-depth comparisons between Figures 4 and 6 shows that the erosion rates are similar at inlet flow velocity of 10 m/s but differs significantly as the velocity is reduced from 10 to 5 m/s and from 5 to 1.0 m/s. At $V_i = 1$ m/s, the erosion rate is negligible at most of the radial locations in the case of the upward flow. The difference in the magnitudes of the erosion rate at low velocity values between the upward and downward flows is attributed to the fact that the influence of

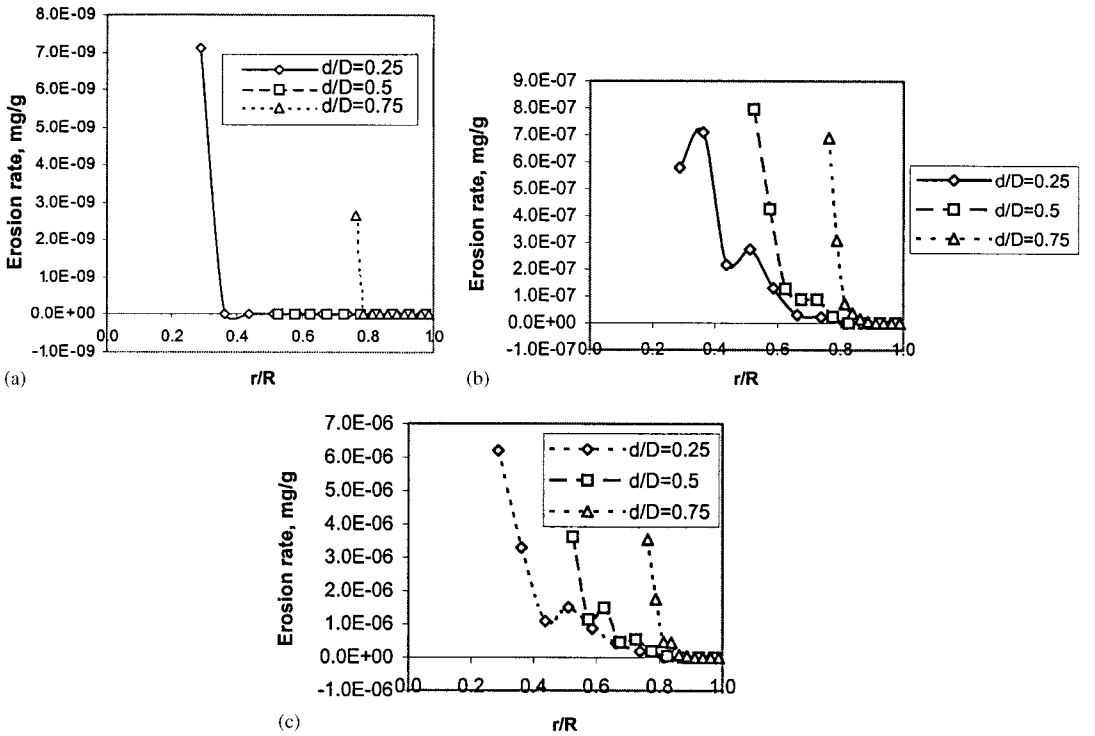

Figure 6. The influence of contraction ratio and inlet flow velocity on the local rate of erosion for the upward flow case, particle diameter = 200 μm: (a) Inlet flow velocity = 1 m/s; (b) inlet flow velocity = 5 m/s; and (c) inlet flow velocity = 10 m/s.

the buoyancy forces is significant in the low velocity range and negligible in the high velocity range.

Figure 7 presents the influence of the inlet flow velocity on the total erosion rate along the surface of the contraction disc at three different contraction ratios. The data of Figure 7 defines a threshold velocity of 1 m/s at which the erosion rate is zero for all the three cases of contraction ratios. In comparison with Figure 5, it is shown that the erosion rates are smaller for the upward flow case in comparison to the downward flow case and, in particular, for the low velocity range where the influence of the buoyancy forces is significant.

4. CONCLUDING REMARKS

Mathematical models for the calculations of the flow velocity field and the motion of the solid particles have been established. These models in addition to models of erosion were used to predict erosion rates under different conditions of inlet flow velocity and pipe contraction ratios. Due to the lack of experimental data the present model was validated through comparison with available calculations. The present results show that the influence of the contraction

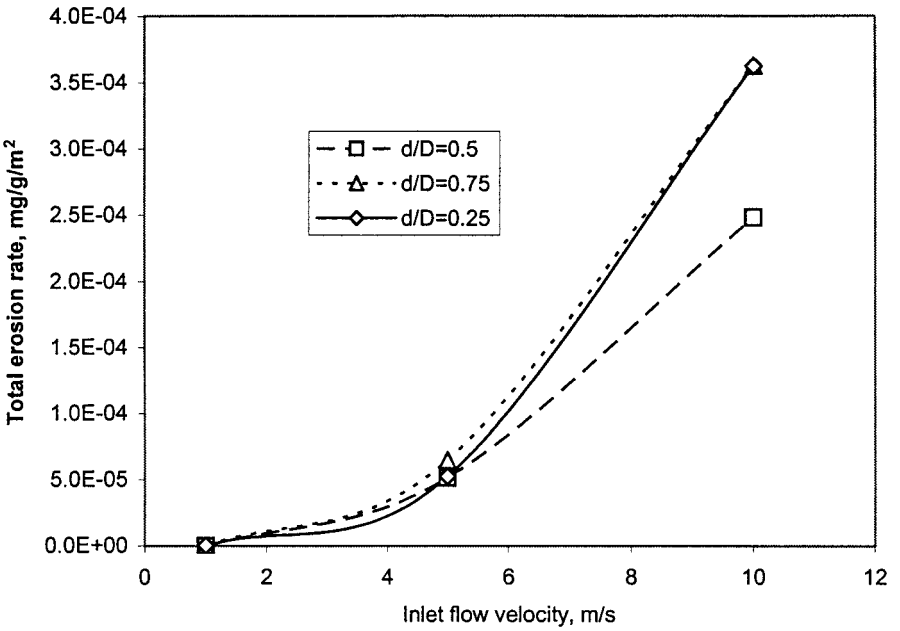

Figure 7. The influence of contraction ratio and inlet flow velocity on the total rate of erosion for the up flow case, particle diameter = 200 μm.

ratio on local erosion is very significant. However, this influence becomes insignificant when the average erosion rates over the sudden contraction area are considered. The results also indicate the significant influence of inlet velocity variations. The influence of buoyancy is significant for the cases of low velocity of the continuous flow.

NOMENCLATURE

A	surface area
b	constant defined in Equation (12)
C_D	drag coefficient
C_μ	constant defined in Equation (4)
C_1	constant defined in Equation (6)
C_2	constant defined in Equation (8)
C_2^*	constant defined in Equation (6)
d	diameter
E	erosion rate, mg/g
F	force
G_k	generation of turbulent kinetic energy

g gravitational acceleration
k turbulent kinetic energy
m_p mass of individual particle
N_p total number of particles being tracked
p pressure
P_n penetration rate
Re_p particle Reynolds number
s sand flow
$\overline{U_j}$ average velocity component
$\underline{u}$ fluid velocity vector
u_j fluctuating velocity component
u_p particle velocity
V_i inlet flow velocity
x_j space co-ordinate
t time

Greek letters

α impact angle
ε dissipation rate of turbulent kinetic energy
μ dynamic viscosity
ρ density
σ_k effective Prandtl number for k
σ_ε effective Prandtl number for ε

Superscripts

. time rate
— time average

Subscripts

D drag
eff effective
lc local
m target material
p particle or near wall node
pg pressure gradient

ACKNOWLEDGEMENTS

The support of King Fahd University of Petroleum and Minerals during this work is acknowledged.

REFERENCES

1. Boulet P, Oesterle B, Andreux R. Comparisons between Eulerian–Eulerian and Eulerian–Lagrangian formulation of a gas–solid suspension flow in a heated pipe. *Proceedings of the 1999 ASME Fluids Engineering Division Summer Meeting*, San Francisco, CA, FEDSM99-7860, 1999.

2. Tsuji Y, Morikawa Y, Shiomi H. LDV measurements of an air–solid two-phase flow in a vertical pipe. *Journal of Fluid Mechanics* 1984; **139**:417–434.
3. Jepson G, Poll A, Smith W. Heat transfer from gas to wall in a gas/solid transport line. *Transactions Institution of Chemical Engineering* 1963; **41**:207–211.
4. Lu QQ, Fontaine JR, Aubertin G. A Lagrangian model for solid particles in turbulent flows. *International Journal of Multiphase Flow* 1993; **19**(2):347–367.
5. Keating A, Nesic S. Particle tracking and erosion prediction in three-dimensional bends. *Proceedings of 2000 ASME Fluids Engineering Summer Meeting*, Boston, MA, 11–15 June, Paper No. FEDSM2000–11249, 2000.
6. Edwards JK, McLaury BS, Shirazi SA. Evaluation of alternative pipe bend fittings in erosive service. *Proceedings of 2000 ASME Fluids Engineering Summer Meeting*, Boston, MA, 11–15 June, Paper No. FEDSM2000–11245, 2000.
7. Wallace MS, Peters JS, Scanlon TJ, Dempster WM, McCulloch S, Ogilvie JB. CFD-based erosion modeling of multi-orifice choke valves. *Proceedings of 2000 ASME Fluids Engineering Summer Meeting*, Boston, MA, 11–15 June, Paper No. FEDSM2000–11244, 2000.
8. Wang J, Shirazi SA, Shadly JR, Rybicki EF. Application of flow modeling and particle tracking to predict sand erosion rates in 90-degree elbows. *ASME Fluids Engineering Division Conference*, San Diego, CA, FED-vol. 236(1), 1996; 725–734.
9. Hanson R, Patel MK. Development of a model to predict the life of pneumatic conveyor bends subject to erosive wear. *Proceedings of 2000 ASME Fluids Engineering Summer Meeting*, Boston, MA, 11–15 June, Paper No. FEDSM2000–11246, 2000.
10. Forder A, Thew M, Harrison D. A numerical investigation of solid particle erosion experienced within oilfield control values. *Wear* 1998; **216**:184–193.
11. Ahlert KR. Effects of particle impingement angle and surface wetting on solid particle erosion on ANSI 1018 steel. *M.S. Thesis*, University of Tulsa, U.S.A., 1994.
12. Shirazi SA, McLaury BS. Erosion modeling of elbows in multiphase flow. *Proceedings of 2000 ASME Fluids Engineering Summer Meeting*, Boston, MA, 11–15 June, Paper No. FEDSM2000–11251, 2000.
13. Patankar SV. *Numerical Heat Transfer and Fluid Flow* (1st edn), Taylor and Francis: London, 1980.
14. Tilly GP. A two-stage mechanism of ductile erosion. *Wear* 1973; **23**:87–96.
15. Ruff AW, Wiederhorn SM. Erosion by solid particle impact. In *Treatise on Materials Science and Technology*, Preece CM (ed.), vol. 16. Academic Press: New York, 1979; 69–125.
16. Davies JE, Stead RJ, Andrews CJ, Richards JR. The airborne particle erosion resistance of a range of engineering materials. *Key Engineering Materials* 1991; **117**:45–52.
17. Habib MA, Attya AE, McEligot DM. Calculation of turbulent flow and heat transfer in channels with streamwise periodic flow. *ASME Journal of Turbomachinery* 1989; **110**:405–411.
18. Versteeg HK, Malalasekera W. *An Introduction to Computational Fluid Dynamics*; *The Finite Volume Method*, Longman Scientific and Technical: London, 1995.
19. Reynolds WC. Fundamentals of turbulence for turbulence modeling and simulation. Lecture Notes for Von Karman Institute, Agard Report No. 755, 1987.
20. Shih TH, Liou WW, Shabbir A, Zhu J. A new k-ε eddy-viscosity model for high Reynolds number turbulent flows—model development and validation. *Computers and Fluids* 1995; **24**(3):227–238.
21. Launder BE, Spalding DB. The numerical computation of turbulent flows. *Computer Methods in Applied Mechanics and Engineering* 1974; **3**:269–289.
22. Benchaita MT, Griffith P, Rabinowicz E. Erosion of metallic plate by solid particles entrained in a liquid jet. *Journal of Engineering for Industry* 1983; **105**:215–222.
23. Shirazi SA, McClaury BS, Shadley JR, Rybicki EF. Generalization of the API RP 14E Guideline for erosive services. *Journal of Petroleum Technology* (Distinguished Author series) 1995; **47**(8):693–698.
24. Morsi SA, Alexander AJ. An Investigation of particle trajectories in two-phase flow systems. *Journal of Fluid Mechanics* 1972; **55**(2):193–208.
25. Haider A, Levenspiel O. Drag coefficient and terminal velocity of spherical and nonspherical particles. *Powder Technology* 1989; **58**:63–70.
26. Li A, Ahmadi G. Dispersion and deposition of spherical particles from point sources in a turbulent channel flow. *Aerosol Science and Technology* 1992; **16**:209–226.
27. Meng H, Vander Geld CWM. Particle trajectory computations in steady non-uniform liquid flows. *ASME Fluids Engineering Division*, vol. 118, FED, 1991; 183–193.
28. Tabakoff W, Wakeman T. Measured particle rebound characteristics useful for erosion prediction. *ASME Paper* 82-GT-170, 1982.
29. Isomoto Y, Nishimura M, Nagahashi K, Matsumura M. Impact angle dependence of erosion by solid particle impact for metallic materials. *Erosion Engineering* 1999; **48**(6):355–361.
30. McLaury BS, Shirazi S. A predicting erosion in straight pipes. *Proceedings of the 1998 ASME Fluids Engineering Division*, Washington, DC, June 21–25, FEDSM 98-5226, 1998.
31. Shirazi SA, Shadley JR, McLaury BS, Rybicki EF. A procedure to predict solid particle erosion in elbows and tees. *Journal of Pressure Vessel Technology* 1995; **117**:45–52.

32. Postletwaite J, Nesic S. Erosion in disturbed liquid/particle pipe flow; effects of flow geometry and particle surface roughness. *Corrosion* 1993; **49**(10):850–859.
33. Finnie I. The mechanism of erosion of ductile metals. *Proceedings of 3rd U.S. National Congress of Applied Mechanics*, Providence, RI, 1958; 527–532.
34. Finnie I, Stevick GR, Ridgely JR. The influence of impingement angle on the erosion of ductile metals by angular abrasive particles. *Wear* 1992; **152**:91–98.
35. Neilson JH, Gilchrist A. Erosion by a stream of solid particles. *Wear* 1968; **11**:111–122.
36. McLaury BS, Wang J, Shirazi SA, Shadley JR, Rybicki EF. Solid particle erosion in long radius elbows and straight pipes. *Society of Petroleum Engineers*, Paper No. SPE 38842, 1997; 977–986.
37. Wang J, Shirazi SA, Shadley JR, Rybicki EF. Application of flow modeling and particle tracking to predict sand erosion rates in 90-degree elbows. *1996 ASME Fluids Engineering Division Conference*, San Diego, CA, vol. 1, 1996; 725–734.
38. Shirazi SA, Shadley JR, McLaury BS, Rybicki EF. A procedure to predict solid particle erosion in elbows and tees. *Journal of Pressure Vessel Technology* 1995; **117**:45–52.

